Detonation regimes in a small-scale RDE

Sylvain Hansmetzger, Ratiba Zitoun, Pierre Vidal
Pprime Institute - UPR3346 CNRS, Department of Fluid, Thermal and Combustion Sciences
ENSMA, 1, avenue Clement-Ader, F86961 Futuroscope-Chasseneuil, France

1 Introduction

For about one century, thrust generation in propulsive devices has been commonly using the isobaric combustion process. However, the detonation process appears to be a promising alternative, mostly because of its higher thermal efficiency [1]. Three types of detonation engine have been considered, Rotating Detonation Engine (RDE), Pulse Detonation Engine (PDE) and Oblique Detonation Wave Engine (ODWE). RDEs can be used in a wide range of flight conditions with a single initial ignition whereas one-cylinder PDEs require high ignition frequencies, and ODWEs operate in narrow interval of Mach numbers. Two geometries of RDE have been considered [2–4]. In the axial type, the chamber is the annular space between coaxial cylinders. In the radial type, the chamber is the space between two disks bounded by a peripheral outer wall. Injection is then made either at the peripheral wall toward center, or from the center wall toward the outer one, with peripheral ejection. In RDE chambers, the detonation velocity, the number of wave fronts, their structure and their amplitude depend on several parameters such as the width and the diameter of the chamber, the mixture composition, the mass flow rate and the injection method. Each of these parameters must be investigated in order to assess its influence on detonation behaviors. Nicholls et al. [5] have presented a feasibility study of a rocket-type RDE. They have obtained a Chapman-Jouguet (CJ) detonation in a few tests, but they have pointed out that injection control was one of the main difficulty to achieve detonation in the chamber. Canteins [6] has designed and operated an axial RDE. He has observed the stable rotation of 1 to 8 simultaneous reactive fronts, depending on the injection conditions and the geometrical configurations. The propulsive performances were evaluated on the basis of thrust and specific impulse measurements. Bykovskii et al. [2, 3, 7] have studied axial and radial RDEs with several chamber geometries and several fuels (Ethylene, Hydrogen) with Air. They have determined a minimal outer diameter of the RDE chamber for detonation propagation as $d_c \approx 40\lambda$, with λ the mean width of the cells that characterize the unstable local structure of the detonation front [11]. Frolov et al. [8] have tested a large-scale hydrogen-air RDE with a 406-mm outer diameter and a 25-mm channel width. They have identified detonation regimes with 1, 2 or 4 fronts and one transient mode with 2 to 1 fronts. Schwer and Kailasanath [9, 10] have developed numerical modelings of rotating detonation fronts in RDEs.

In this work, we describe an experimental study of the detonation regimes in a small, axial-type RDE. The study focuses on the effects of the chamber inner geometry on the detonation regimes as functions of the mass flow rate $\dot{m}$ and of the mean width λ. The inner geometry of the chamber was varied by considering a long and a short cylindrical kernel, and a short conical kernel. The cell mean width λ was varied by considering mixtures of ethylene (C_2H_4) and enriched air (Air$^+$) with several nitrogen dilutions ($\beta = \frac{[N_2]}{[N_2]+[O_2]}$) and equivalence ratios ER. The reference values for λ were taken from the Caltech Database [13] and are given in Table 1 as function of β and ER.

β \ ER	0.8	1	1.2
79%	67 mm	27 mm	26 mm
50%	8 mm	3 mm	3 mm
0%	1.5 mm	0.6 mm	0.6 mm

Table 1: Mean width of detonation cells in Ethylene/Air$^+$ compositions. ER: equivalence ratio, β: N_2 dilution, $P_0 = 1$ atm and $T_0 = 300$ K.

2 Experimental set-up

Figure 1 and Figure 2 show some views of our experimental set-up and a scheme of the three kernels of the annular chamber, respectively. The outer wall of the chamber has a 70-mm diameter d_0 and a 90-mm length L (Fig. 1b, top). The diameter of the long and of the short cylindrical kernels is $d_i = 50$ mm, the short conical kernel is converging, with diameter decreasing from d_i at the chamber entry to $d_e = 42$ mm (i.e., opening angle $\alpha = 7.6\,^\circ$and surface expansion ratio $S/S_0 = 1.3$). The long cylindrical kernel has the same length as the chamber ($L = 90$ mm) and the short, cylindrical or conical, kernels are 30-mm long (i.e., 35% of L). The channel width is here defined by $e = (d_0 - d_i)/2$ and is equal to 10 mm.

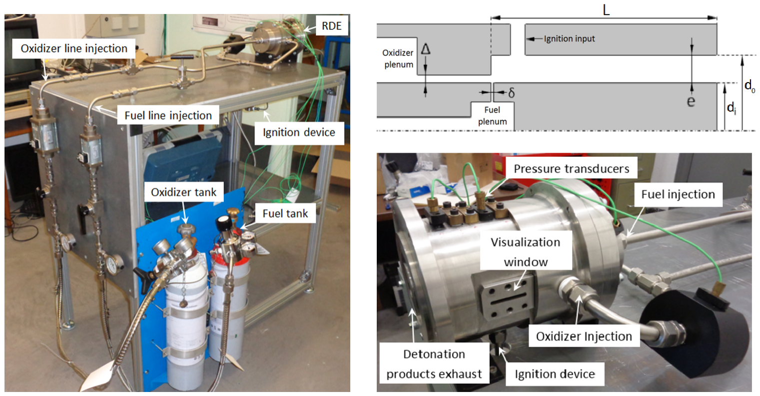

(a) (b)

Figure 1: (a) : Experimental set-up; (b) : RDE sectional view (top), General view of the chamber (bottom)

Two injection plenums, one for the fuel (C_2H_4), and one for the oxidizer (Air$^+$), are used to supply the chamber. Each gas is stored in a 5-liters high-pressure tank (Fig. 1a). The fuel is injected radially through a circular spacing with adjustable thickness δ (~ 0.3 mm) and the oxidizer through a 0.5-mm ring (Δ) tangent to the kernel. Mixing is made at the intersection of the plenums exits, at the chamber entry-end (Fig. 1b, top).

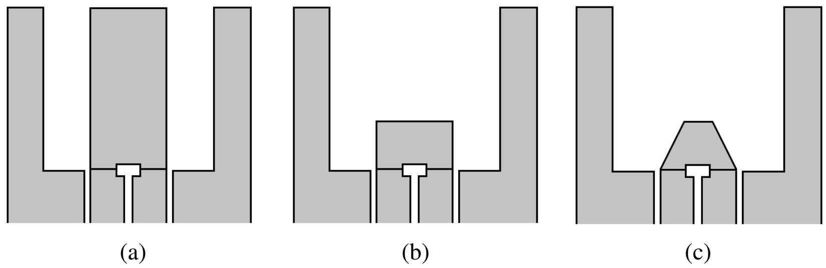

Figure 2: The three configurations of the chamber: long cylindrical kernel (a), short cylindrical kernel (b), short conical converging kernel (c)

A regulator valve is used to control the stagnation pressures and the mass flow rates in the supply lines of the fuel and of the oxidizer. The mass flow rates are determined by measuring the weights of the tanks before and after the test. Eight Kistler pressure transducers (603B), P1 to P8, are positioned on the chamber outer wall, 5 at the chamber top, along a parallel to the axis (e.g., Fig. 1b, bottom), and 3 along the circumference that contains the second transducer (P2) on the chamber top line. A Kistler pressure transducer is positioned in each plenum to measure the stagnation pressures of the fuel and of the oxidizer,Pfuel and Poxd, respectively. Visualizations are made through a window on the outer wall and at the exit-end of the chamber. A high-speed camera is used with frequencies from 50 to 120 kHz and exposure times from 7.5 µs to 250 ns. The ignition device is an 8-mm inner diameter tube with an automotive spark plug and a Shchelkin spiral at the ignition end. The other end is connected radially to the outer wall of the chamber, a few millimeters after the injection ring (Fig. 1b, top). The ignition tube is filled with the stoichiometric mixture $C_2H_4+3O_2$, and a detonation is generated by means of a Deflagration-to-Detonation Transition process. This detonation is then transmitted radially to the chamber and used to initiate the detonation of the premixed gas $C_2H_4+Air^+$ injected in the chamber.

3 Results

Figures 3 and 4 summarize the results for the three configurations of kernels shown in Figure 2. Figure 3a shows the detonation velocity ratio D/D_{CJ} as function of the equivalence ratio ER, Figure 3b shows the ratio e/λ of the chamber width e to the cell mean width λ as function of the mass flow rate $\dot{m}$. Figure 4 shows the pressure signals for each kernel configuration. The reference CJ velocities D_{CJ} were calculated with the GASEQ thermodynamic-equilibrium code [14] for each equivalence ratio ER and each dilution β at atmospheric conditions.

We first have studied the combustion modes with the long cylindrical kernel (Fig. 2a, Configuration 1). We have obtained two combustion modes, specifically a two-fronts detonation regime and a volumetric combustion mode (Fig. 3, semi-open and open green diamonds, respectively). No one-front detonation regime could be installed in our intervals of mass flow rate and dilution. We have considered equivalence ratios in the interval [0.84 - 1.5] and the three Nitrogen dilutions 50%, 30% and 0% (i.e, pure Oxygen), which give ratios e/λ in the intervals [1.8 - 4], [3 - 12] and [8.5 - 22], respectively. The two-fronts detonation regime shows two fronts propagating in opposite directions. Their collisions occur at positions 90°and 270°-with position 0°at the bottom of the chamber- as indicated by the triggering sequence [P2 - P8 - P2] of transducers P2 and P8, and by the pressure peak measured by transducer P8, at position 270°(Fig. 4a). The volumetric combustion mode is the situation for which the pressure transducers trigger quasi-simultaneously and no shock front is observed.

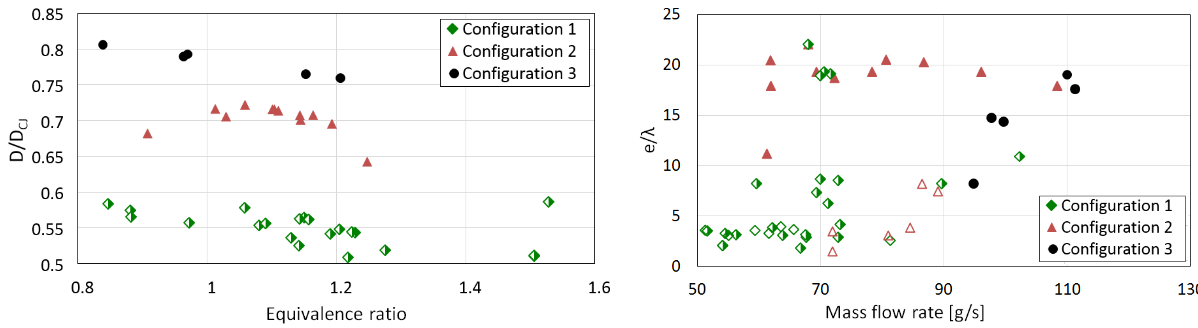

(a) (b)

Figure 3: Distribution of combustion modes : (a) Detonation velocity ratio vs. equivalence ratio; (b) channel width-to-cell width ratio (e/λ) vs. mass flow rate. The full, semi-open and open symbols denote the one-front rotating and the two-fronts detonation regimes, and the volumetric combustion mode for each configuration, respectively.

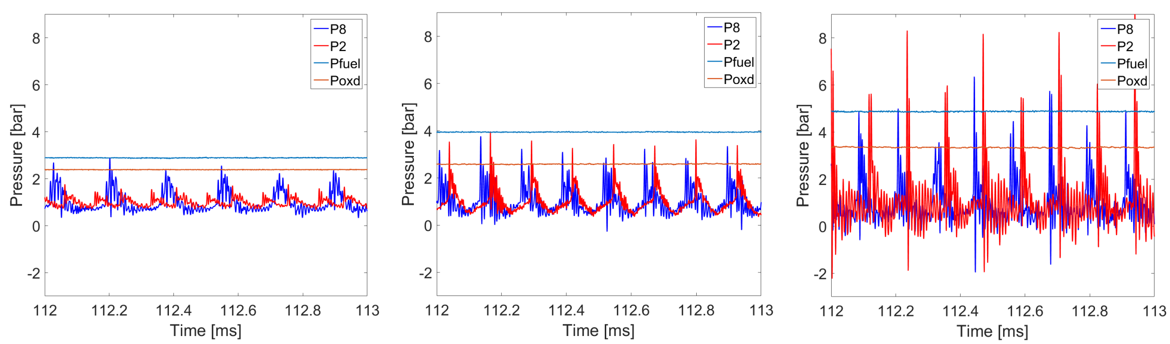

(a) (b) (c)

Figure 4: Pressure signals in the chamber (transducers P8 and P2) and in the plenums (transducers Pfuel and Poxd) for Configurations 1 (a), 2 (b) and 3 (c). Mixture : ER $C_2H_4 + 3O_2$. Mass flow rate : 60 g/s (a), 72 g/s (b) and 110 g/s (c). Equivalence ratio (ER) : 1.12 (a), 1.16 (b) and 1.15 (c).

The volumetric combustion mode was only obtained for the 50% dilution and for $e/\lambda < 4$. The two-fronts counter-rotating detonation regime was obtained for mass flow rates up to 105 g/s and e/λ up to 22. For this configuration, the transition value of e/λ between the two-fronts and the volumetric modes is $\sim$ 4 - 5. For the two-fronts detonation regime, the peak pressure is about 2 bar for the 50% dilution and 3 bar (Fig. 4a) for pure oxygen oxidizer, and the measured velocities range between 51% and 60% of the Chapman-Jouguet value D_{CJ} (Fig. 3a).

We then have studied the combustion modes with the short cylindrical kernel (Fig. 2b, Configuration 2). We have obtained two combustion modes, specifically a one-front detonation regime and a volumetric combustion mode (Figure 3, full and open red triangles, respectively). We have considered equivalence ratios in the interval [0.9 - 1.25] and the same three nitrogen dilutions (50%, 30% and 0%) as for Configuration 1 (long cylindrical kernel), which give ratios e/λ in the intervals [1.5 - 3.9], [7.4 - 8.2] and [11.2 - 20.5], respectively. The one-front detonation regime was obtained with pure oxygen, and the volumetric combustion mode was obtained with the 50% and 30% dilutions. Also, the transition value $e/\lambda \sim 9$ - 10 between the volumetric combustion mode and the one-front detonation regime is larger than in Configuration 1. The measured velocities range between 65% and 72% of the CJ velocity (Fig. 3a) and the pressure peaks between 4 and 5 bar (Fig. 4b). The ratio D/D_{CJ} appears to present a maximum for the equivalence ratio $ER = 1.06$ which, as matter of fact, corresponds to the value where the mean width of detonation cells λ is the smallest.

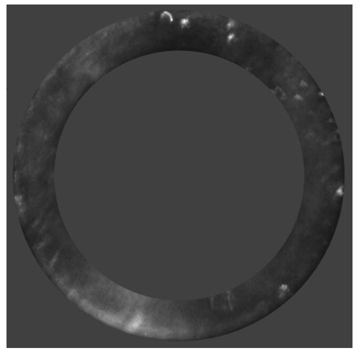

Figure 5: Head-on snapshot of the one-front detonation regime (Configuration 2). $ER = 1.07$, $\dot{m} = 73$ g/s, $\beta = 0$. Recording speed : 120 kHz.

The high-speed camera visualizations confirm the information on the combustion modes given by the pressure transducers. Figure 5 is an example of a head-on snapshot of the one-front detonation regime. The front is rotating counter-clockwise and located at about -20°on the snapshot. We observe that the front is more luminous closer to the outer wall than to the kernel. The luminous dots are burning particles of the silicon layers used to protect the pressure transducers and eroded by the successive passages of the detonation front.

We finally have studied the combustion modes with the short converging kernel (Fig. 2c, Configuration 3). We have obtained a one-front detonation regime (Figure 3, full black circles). We have considered equivalence ratios in the interval [0.8 - 1.2] and pure oxygen as the oxidizer, which give ratios e/λ in the interval [8.2 - 19]. The measured velocities range between 76% and 80% of the CJ velocity (Fig. 3a) and pressure peaks between 7 and 8 bar (Fig. 4c), which constitutes a marked improvement compared with the values obtained with the kernel configurations 1 and 2.

4 Discussion and conclusion

In our conditions, the chamber inner geometry was found to have a significant influence on the combustion modes. The use of short kernels, here about 35% of the chamber length, considerably improves the detonation properties of our non-diluted mixtures. Similar observations have been recently reported by Zhang et al. [12]. In our conditions, the best performances were obtained with a short, conical converging kernel. The physical interpretation is that too long kernels hinder the evacuation of the burnt gases, and so the actual mixture in the chamber does not contain enough fresh gases for an optimum detonation process. It is an open question whether a minimum kernel length exists that would provide the best performances in our conditions of injection. As a matter of fact, determining the best inner geometry for a RDE chamber and the actual wave configuration is still a difficult issue. Nevertheless, the present work demonstrates the stable operability of a small RDE at low mass flow rates.

In future works, we will continue to investigate the enhancement of detonation properties in our RDE depending on the chamber inner geometry, the mixture dilution and the mass flow rate. Special attention will be given to characterizing the position of the combustion zone in the chamber and the wave configuration by means of high-speed camera visualizations.

5 Acknowledgment

This work is part of the CAPA research program on Alternative Combustion Modes for Air-breathing Propulsion supported by SAFRAN, MBDA and the French National Research Agency (ANR).

References

[1] Voitsekhovskii BV, Mitrofanov VV, Topchiyan ME, (1969), Structure of the detonation front in gases (survey), Combustion Explosion and Shock Waves, 3: 267.

[2] Bykovskii FA, Vasilev AA, Vedernikov E, Mitrofanov VV, (1994), Explosive combustion of a gas mixture in radial annular chambers, Combustion Explosion and Shock Waves, 30: 510.

[3] Bykovskii FA, Mitrofanov V, Vedernikov E, (1997), Continuous detonation combustion of fuel-air mixtures, Combustion Explosion and Shock Waves, 33: 344.

[4] Kasahara J, (2015), Rotating Detonation Rocket Engine Experiments, IWDP Beijing.

[5] Nicholls JA, Cullen RE, Ragland KW, (1966), Feasibility studies of a rotating detonation wave rocket motor, Journal of Spacecraft and Rockets, American Institute of Aeronautics and Astronautics, 3: 893.

[6] Canteins G, (2006), Etude de la detonation continue rotative, Application a la propulsion, PhD thesis, Universite de Poitiers.

[7] Bykovskii FA, Zhdan SA, Vedernikov EF, (2006), Continuous Spin Detonations, Journal of Propulsion and Power, American Institute of Aeronautics and Astronautics, 22: 1204.

[8] Frolov S, Aksenov V, Ivanov V, Shamshin I, (2015), Large-scale hydrogen-air continuous detonation combustor, International Journal of Hydrogen Energy, Elsevier, 40: 1616.

[9] Schwer D, Kailasanath K, (2010), Numerical investigation of rotating detonation engines, AIAA paper, 6880: 2010.

[10] Schwer D, Kailasanath K, (2011), Numerical investigation of the physics of rotating-detonation-engines, Proceedings of the Combustion Institute, Elsevier, 33: 2195

[11] Knystautas R, Lee JH, Guirao CM, (1982), The critical tube diameter for detonation failure in hydrocarbon-air mixtures, Combustion and Flame, 48, 63-83.

[12] Zhang H, Liu W, Liu S, (2016), Effects of inner cylinder length on H2/air rotating detonation, International Journal of Hydrogen Energy, 41, 13281-13293.

[13] Kaneshige M, Shepherd JE, (1997), Detonation database.

[14] Morley C, (2005), Gaseq: a chemical equilibrium program for Windows, http://www.gaseq.co.uk.